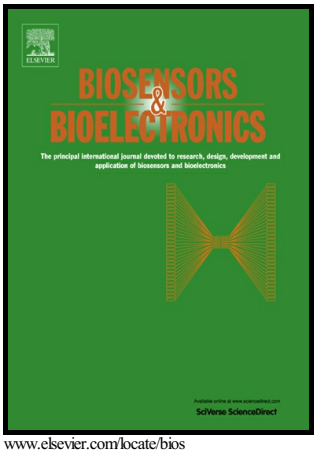

www.elsevier.com/locate/bios

Core-shell iron oxide-layered double hydroxide: High electrochemical sensing performance of H_2O_2 biomarker in live cancer cells with plasma therapeutics

Muhammad Asif, Hongwei Liu, Ayesha Aziz, Haitao Wang, Zhengyun Wang, Muhammad Ajmal, Fei Xiao, Hongfang Liu

PII: S0956-5663(17)30375-5
DOI: http://dx.doi.org/10.1016/j.bios.2017.05.057
Reference: BIOS9770

To appear in: *Biosensors and Bioelectronic*

Received date: 16 March 2017
Revised date: 12 May 2017
Accepted date: 31 May 2017

Cite this article as: Muhammad Asif, Hongwei Liu, Ayesha Aziz, Haitao Wang, Zhengyun Wang, Muhammad Ajmal, Fei Xiao and Hongfang Liu, Core-shel iron oxide-layered double hydroxide: High electrochemical sensing performanc of H_2O_2 biomarker in live cancer cells with plasma therapeutics, *Biosensors an Bioelectronic,* http://dx.doi.org/10.1016/j.bios.2017.05.057

Core-shell iron oxide-layered double hydroxide: High electrochemical sensing performance of H_2O_2 biomarker in live cancer cells with plasma therapeutics

Muhammad Asif, Hongwei Liu, Ayesha Aziz, Haitao Wang, Zhengyun Wang, Muhammad Ajmal, Fei Xiao*, Hongfang Liu*

Key Laboratory for Large-Format Battery Materials and System, Ministry of Education, Hubei Key Laboratory of Material Chemistry and Service Failure, School of Chemistry and Chemical Engineering, Huazhong University of Science and Technology, Wuhan, 430074, P. R. China.

E-mail: liuhf@mail.hust.edu.cn

E-mail: xiaofei@hust.edu.cn

***Corresponding authors**

Abstract

In this work, we develop a new type of multifunctional core-shell nanomaterial by controllable integration of CuAl layered double hydroxides (LDHs) over the surface of iron oxides (Fe_3O_4) nanospheres (NSs) to fabricate (Fe_3O_4@CuAl NSs) hybrid material with interior tunability of LDH phase and explore its practical application in ultrasensitive detection of emerging biomarker, *i.e.*, H_2O_2 as cancer diagnostic probe. In addition, atmospheric pressure plasmas (APPs) have also been used as potential therapeutic approach for cancer treatment. Due to the synergistic combination of p-type semiconductive channels of LDHs with multi-functional properties, unique morphology and abundant surface active sites, the Fe_3O_4@CuAl NSs modified electrode exhibited attractive electrocatalytic activity towards H_2O_2 reduction. Under the optimized conditions, the proposed biosensor demonstrated striking electrochemical sensing performances to H_2O_2 including linear range as broad as 8 orders of magnitude, low real detection limit of 1 nM (S/N=3), high sensitivity, good reproducibility and long-term stability. Arising from the superb efficiency, the electrochemical biosensor has been used for *in vitro* determination of H_2O_2 concentrations in human urine and serum samples prior to and following the intake of coffee, and real-time monitoring of H_2O_2 efflux from different cancer cell lines in normal state and after plasma treatment. We believe that this novel nano-platform of structurally

integrated core-shell nanohybrid materials combined with APPs will enhance diagnostic as well as therapeutic window for cancer diseases.

Graphical abstract

Keywords: Fe_3O_4 nanospheres; p-type layered double hydroxide; electrochemical biosensor; hydrogen peroxide detection; live cells

1. Introduction

Hydrogen peroxide (H_2O_2), with the ongoing need of gigantic investigation, has emerged as rapidly increasing current research themes and fascinated great enthusiasm of researchers due to its extreme biological significance. It is worth mentioning that H_2O_2 plays a vital role in cell proliferation, cell death, response to chronic diseases and intracellular signaling transduction (Ai et al., 2009; Maji et al., 2014). A key feature of studying H_2O_2 in living organisms is to ensure that its concentration in cellular compartments should be in physiological range of 1 nM to 0.5 μM in all mammals (Weinstain et al., 2014; Zhu et al., 2016). Recent biomarker based cancer diagnosis has drawn extensive attention of scientists because of their high reliability, sensitivity and simplicity. Studies have profiled the cellular functions associated with endogenous H_2O_2 efflux in living cells are emerging recognized biomarker for cancer diagnostics, principally endowing the measurement facilities with conventional assays (Xi et al., 2016). Considering the practical significance of H_2O_2 in biological systems, precise detection of cellular H_2O_2 is critically essential to avoid lethal attacks of oxidative stress, neurodegenerative disorders, tumor growth (Yu et al., 2015), and further offering reliable diagnosis of destructive physiological conditions.

To date, among the various developed analytical techniques, electrochemical transducer based biosensors have attracted considerable attention because of their high sensitivity, selectivity, portability and aptitude for real-time *in vitro* and *in vivo* tracking of H_2O_2 efflux (Luo et al., 2009; Yin et al., 2014). The natural enzyme based electrochemical biosensors are found to be more reliable, sensitive and quick responsive for detection of H_2O_2 than conventional calorimetric method (Ding et al., 2010) owing to profound specificity of enzymes for catalytic

H_2O_2 reduction (Li et al., 2011; Wu et al., 2011). However, the enzyme modified electrode suffers from instability, complication in immobilization and high cost (Xu et al., 2015; Yuan et al., 2014), these natural enzymes are not readily available to be used under such electrochemical conditions for detection of H_2O_2. Therefore, the development of non-enzymatic H_2O_2 biosensors based on direct electrocatalytic redox of H_2O_2 is highly desirable. Particularly, several non-noble metals, such as Cu, Mn, Fe and their oxides with unique nanostructures have exhibited large surface area, quick electron transfer, enhanced electrocatalytic abilities and high stability (Ganesan and Lee, 2005), which have been considered to be even superior to the rare, and expensive noble metals, and hold great promise in H_2O_2 electrocatalysis systems.

Layered double hydroxides (LDHs), a class of inorganic materials with brucite type layered structure and intriguing properties, have been extensively explored in catalysis, cancer therapy (Senapati et al., 2016), separation and sensors due to their distinctive features of typical memory effect, excellent thermal stability and inherent electrocatalytic capabilities (Asif et al., 2015). This is originated from the p-type semiconductive channels of LDHs, which consist of high ordered alternative configuration of M^{2+} and M^{3+} cations and charge complimentary anions in the host layers. In virtue of topotactic transformation, large -OH surface functional groups and excessive positive charge on LDHs, LDHs ensure marvelous intercalation features to form multilamellar hierarchical morphology. Especially, biocompatible non-noble metal nanoparticles like Fe_3O_4 (Williams et al., 2016) intercalated LDH materials have drawn considerable interest of researchers to explore them as an alternative electrocatalyst in the field of electrochemistry (Wang et al., 2012).

Herein, we report structurally integrated core-shell Fe_3O_4@CuAl nanospheres (NSs) with Fe_3O_4 NSs as the core and CuAl LDHs as the shell, and explore their practical application as dedicated electrocatalyst for H_2O_2 reduction and its application in sensitive and selective detection of H_2O_2 in different real samples. A series of Fe_3O_4@CuAl NSs have been synthesized by facile hydrothermal and co-precipitation approaches, which offer the benefits of inexpensive, simple processing, controlled size and enhanced loading capacity. The as-obtained hierarchical assembly exhibits enhanced catalytic ability for the reduction of H_2O_2 by interfacial collaboration between Fe_3O_4@CuAl and the fractional charge transfer between p-type conductive LDHs and Fe_3O_4 at nanoscale interface. Benefits from large specific surface area, charge transfer aptitude and availability of gigantic surface active sites, Fe_3O_4@CuAl NSs demonstrated excellent

electrochemical sensing performance for H_2O_2 detection, such as broad linear range, very low real detection limit of 1 nM. The practical application of Fe_3O_4@CuAl NSs used in modifying electrode for *in vitro* sensitive detection of the endogenous H_2O_2 in human serum, urine as well as cellular H_2O_2 triggered from different cancer cells.

Cancer has become growing cause of mortalities worldwide (Chen et al., 2016; Xi et al., 2016; Xi et al., 2015). Despite of countless struggles, the art of potential early cancer detection and therapeutic modalities bear several limitations in clinical examinations, histopathology, imaging mammography and terrible side effects of therapeutic anticancer drugs as well as their high cost (Cardoso et al., 2016; Liu et al., 2016). An accumulated exposure to radiations led by mammography and its insufficient sensitivity, driving the patients into histopathology which is consequently an invasive approach, when the disease is grown (Yahalom et al., 2013). Therefore, substantial advances in technologies for non-invasive, economical and reliable early cancer screening, prognostic evidences and effective therapeutic options are urgently needed.

The goal of our study is not only focused on developing novel material based biosensing platform for cancer diagnosis, but also on uncovering a challenging therapeutic approach for *in vitro* treatment of cancer. Considering the enhanced plasma chemistry of atmospheric pressure plasmas (APPs), a brand new plasma medicines have been extensively studied for novel biological applications such as sterilization, inactivation of bacteria (Von Woedtke et al., 2014), wound healing (Keidar, 2012), and cancer therapy (Tanaka et al., 2015). In this study, we also have established a plasma source with plasma plume carrying a highest current of around 300 mA to investigate the role of charged species in cancer therapy. This elegant approach involves indirect plasma therapy of cancer along with plasma treated solutions containing cancer cells which is termed as plasma activated medium (PAM). With high therapeutic efficacy, plasma treatment of cancer would contribute efficiently to enhance therapeutic window.

2. Experimental section

2.1. Fabrication of nanospheres

Core-shell Fe_3O_4@CuAl NSs were synthesized by a facile hydrothermal and co-precipitation method as shown in Fig. 1A. In the first step, Fe_3O_4 NSs were synthesized by means of modified solvothermal approach. Typically, 2.7 g of $FeCl_3.6H_2O$ were dissolved in 100

ml of ethylene glycol under vigorous stirring along with the addition of 7.2 g sodium acetate. The resulting mixture was kept in Teflon-lined stainless-steel autoclave and heated up to 200 °C. After proceeding 8 h of reaction, the autoclave was allowed to cool down naturally at room temperature. The resulting black product was separated and sequentially washed with ethanol several times and dried at 60 °C under vacuum overnight.

Second, 50 mg of Fe_3O_4 NSs were thoroughly dispersed in 50 ml of water/methanol ($V_{water}/V_{methanol}$=1:1) solution with ultrasonic agitation for 20 min to make it homogeneous. An alkaline solution of 50 ml ($V_{water}/V_{methanol}$=1:1) containing 0.30 g Na_2CO_3 and 0.46 g NaOH was added drop wise to the above solution under vigorously mechanical stirring to obtain pH 10. Another 50 ml ($V_{water}/V_{methanol}$=1:1) mixed suspension of 4.5 mM $Cu(NO_3)_3 \cdot 3H_2O$ and 1.5 mM $Al(NO_3)_3 \cdot 9H_2O$ was added dropwise to the above suspension under vigorous stirring while keeping pH constant at 10 by simultaneously adding same alkaline solution. The resulting suspension was aged under strong mechanical stirring at 65 °C in water bath for 24 h. The as-obtained product was separated by magnet, washed several time with deionized water of pH 7 and kept at 60 °C overnight Fe_3O_4@CuAl NSs. Similarly, CuAl LDHs was also synthesized using same concentrations of $Cu(NO_3)_3 \cdot 3H_2O$ and $Al(NO_3)_3 \cdot 9H_2O$. Finally, 5 µL of the as-prepared Fe_3O_4@CuAl NSs suspension (3 mg mL-1) was casted on the surface of thoroughly polished GCE and dried at ambient temperature, and Fe_3O_4@CuAl NSs modified GCE (Fe_3O_4@CuAl/GCE) was obtained. Fe_3O_4 NSs/GCE and CuAl/GCE were also prepared through the same procedure.

2.2. In-vitro plasma treatment of living cells

To explore the therapeutic effects of charged particles, different cancer cells in 6-well plate were treated directly by plasma plume. A copper wire of 2 mm diameter inserted in 4 cm long quartz tube with one end closed was used as high voltage (HV) electrode. Then this HV electrode was inserted in 6 mm diameter hallow barrel of syringe along with injecting helium gas in hallow barrel as working gas and HV electrode pulsed dc voltage was applied to generate plasma. The generated plasma plume could approximately be 6 cm in length. The cells were placed under plasma plume with adjustable distance of 2 cm between plasma jet nozzle and upper surface of medium in 6-well plate and irradiated for 1 min and 2 min. The cell cultured plate was kept in incubator for 24 h at 37 °C after plasma treatment (Kaushik et al., 2016).

3. Results and discussion

3.1. Characterization of Fe_3O_4@CuAl NSs

The specific surface area of as-prepared Fe_3O_4@CuAl NSs along with percent loading of copper was measured by Brunauer-Emmett-Teller (BET) method, which shows that the surface area increases as Cu content increases in Fe_3O_4@CuAl NSs and attains the maximum surface area of 50.66 m^2 g^{-1} at an intermediate loading of 18.96% of copper (Supporting table S1). Possibly, higher content of Cu results in weak crystallization of LDH materials on the surface of core due to the formation of Cu oxides such as Cu_2O, which caused the decrease of surface area (Asif et al., 2017). The variation in surface area of various samples is possibly due to different stacking modes of CuAl LDH layers.

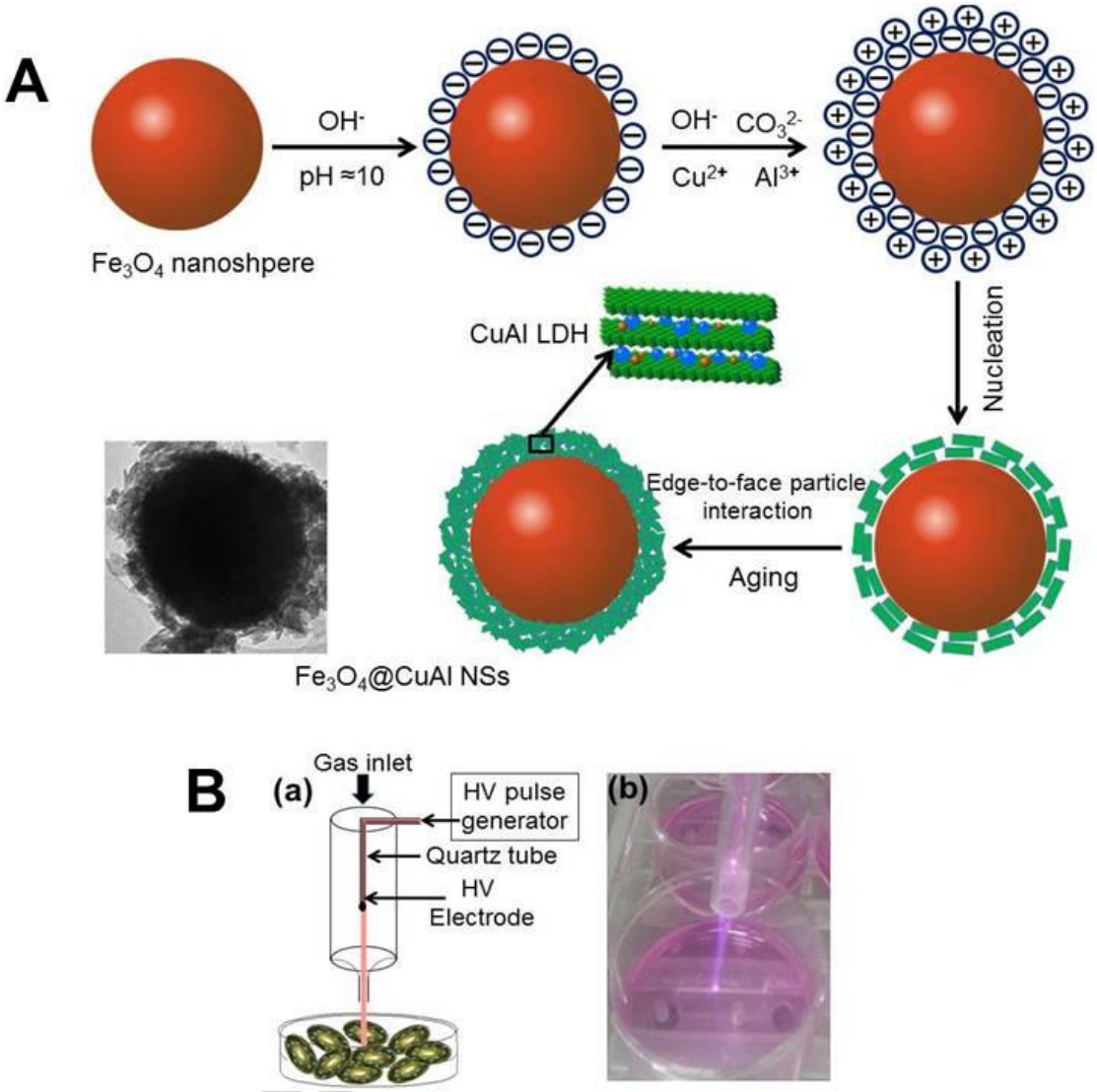

Fig. 1. (A) Flow chart of the synthesis mechanism of Fe_3O_4@CuAl NSs. (B) Schematic representation of experimental setup for direct irradiation of cancer cells (a), photograph of plasma jet device for direct irradiation of cancer cells (b).

The morphology and analytical performances of Fe_3O_4@CuAl NSs with 18.96% of copper loading have further been investigated. The concentration ratio of metallic salts and Fe_3O_4 NSs were adjusted to get different morphologies and size of LDH shell. At low concentration ratio, LDH shell established an even distribution of very small CuAl platelets on Fe_3O_4 core (Fig. S1A). By increasing the ratio of metallic salts and Fe_3O_4 NSs, a very thick layer of LDH shell was obtained due to the agglomeration of CuAl platelets, which entirely covers the whole surface of Fe_3O_4 NSs. After certain intermediate ratio of metallic salts and Fe_3O_4 NSs, the

entire core of Fe_3O_4 NSs is seemed to be buried completely in LDH platelets like shells (Fig. S1B). Fig. 2 shows the SEM and TEM images of as-synthesized Fe_3O_4 and Fe_3O_4@CuAl core-shell nanospheres. It is observed that Fe_3O_4 particles show smoothed surface, nearly monodispersed spherical structure and uniform size with mean diameter of 300 nm (Fig. 2A, 2B and 2E). After being coated by CuAl LDH, the surface of Fe_3O_4@CuAl NSs becomes rough as compared with pristine Fe_3O_4, which is due to the assembly of almost horizontally along with vertically oriented platelets like LDH shells (Fig. 2C). The higher magnification confirms the hydrotalcite like typical stacked layers of CuAl LDHs (Yan et al., 2015), (Fig. 2D). The unique preparation process by adjusting pH at 10 enriches the surface of Fe_3O_4 with negative charge and particular stirring speed, which facilitates the growth of LDH layers on surface of Fe_3O_4 NSs to construct core-shell morphology. The TEM image in Fig. 2F presents the flowerlike Fe_3O_4@CuAl NSs with typical core-shell structure constructed by a compact core of 300 nm in diameter and low density horizontally oriented LDH shell, and thickness of shell is around 40 nm (Fig. 2G). The HRTEM image in Fig. 2H shows that LDH phase has a lattice fringe with d-spacing of 0.25 nm, which is well matched with (111) crystal plane of XRD and can be indexed to CuO with monolithic texture (Ko et al., 2014).

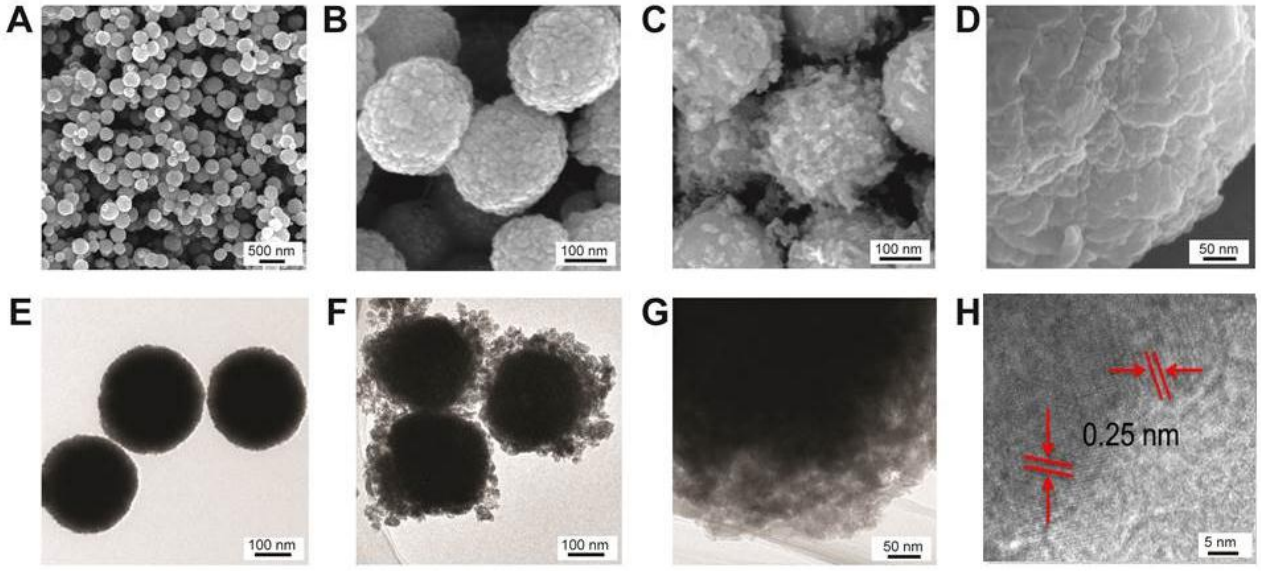

Fig. 2. (A) and (B) SEM images of Fe_3O_4 nanospheres, (C) and (D) SEM images of Fe_3O_4@CuAl NSs with different magnification. (E) TEM images of Fe_3O_4 nanospheres, (F) and (G) Fe_3O_4@CuAl NSs with different magnification. (H) HRTEM image of the CuAl LDH shell with fringe spacing of 0.25 nm.

XPS characterization was further employed to investigate the element composition, and metallic configuration of Fe_3O_4@CuAl NSs. A wide scan spectrum as presented in Fig. 3A shows the distinct peaks assigned to Cu 2p, Fe 2p and Al 2p along with two predominant peaks of carbon and oxygen corresponding to charge complementary hydroxyl and carbonate ions existing in between LDH layers. Fig. 3B exhibits the core level spectrum of Fe 2p, which is further deconvoluted into couple of peaks Fe $2p_{3/2}$ and Fe $2p_{1/2}$ at 710.46 eV and 724.31 eV, respectively. Moreover, Fe 2p spectrum of Fe_3O_4@CuAl NSs shows a weaker peak centered at 710.46 eV correspond to Fe $2p_{3/2}$ for Fe^{3+} species as compared to Fe_3O_4, most probably due to its less intensity as well as horizontal intercalation of platelet like multilamellar shell of CuAl LDH on the surface of Fe_3O_4 core (Song et al., 2010). Both samples contain mixed phase of Fe^{2+} and Fe^{3+} because two deconvoluted peaks of Fe $2p_{3/2}$ appeared at 710.2 eV and 712.1 eV (Wang et al., 2016). The interaction between core and shell influenced the oxidation states of metals which arises the possibility of Cu-O-Fe linkages. Fig. 3C shows the core fitting peaks of Cu $2p_{3/2}$ and Cu $2p_{1/2}$ originated at 932.1 eV, 952.4 eV and 934.2 eV, 954.3 eV, corresponding to Cu^{+} and Cu^{2+} species. Two satellite peaks at around 742 eV and 762 eV are the fingerprint of CuO phase with d^9 electronic configuration (Al-Gaashani et al., 2011; Shen et al., 2015).

Fig. 3D exhibits the typical XRD pattern of Fe_3O_4, CuAl LDH and Fe_3O_4@CuAl NSs. After in situ growth of LDH shell on Fe_3O_4 core, the superimposition reflections of both phases have been shown by XRD pattern. The typical crystal reflections of (003), (006) and (009) appear at 2θ value of 11.2°, 23.1° and 34°, respectively, which are attributed to layered rhombohedral structure of LDH (Han et al., 2015). The crystallographic plane of (111) at 38.90° collapsed with a typical LDH plane of (015), can be attributed to CuO phase in LDHs. The crystal peaks of (220), (311), (400), (511) and (440) at 2θ value of 30.2°, 35.52°, 43.13°, 57.2° and 62.52° respectively are credited to Fe_3O_4 phase.

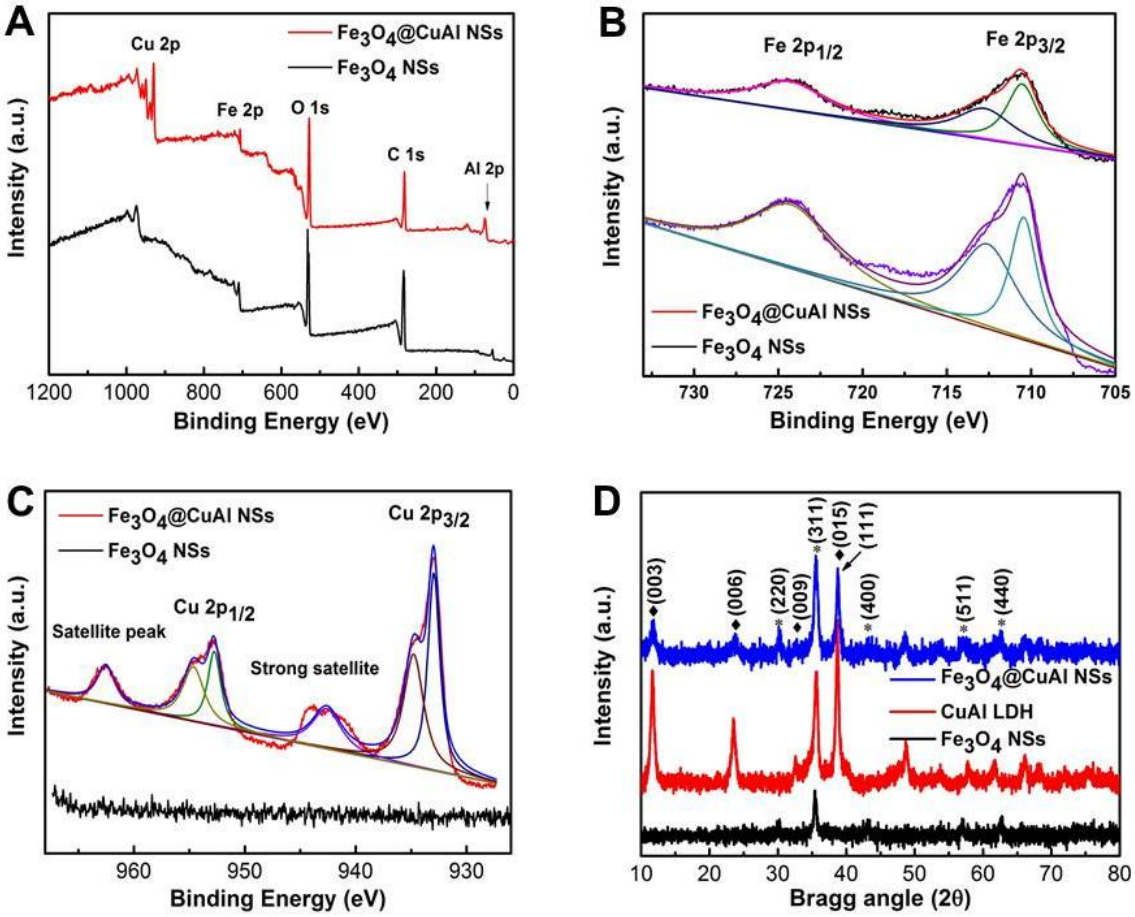

Fig. 3. (A) Wide scan XPS survey spectra, (B) Fe 2p Core level XPS spectra, (C) Cu 2p Core level XPS spectra of Fe_3O_4@CuAl NSs and Fe_3O_4 NSs, (D) XRD patterns of Fe_3O_4@CuAl NSs, CuAl LDHs and Fe_3O_4 NSs (from upper to lower).

3.2. Electrochemical properties of Fe_3O_4@CuAl/GCE

To investigate interfacial properties of electrode surface modified by Fe_3O_4, CuAl LDH and Fe_3O_4@CuAl NSs, EIS has been performed with $[Fe(CN)_6]^{3-/4}$ redox probe, as shown in Fig. 4A. And the inset is the Randle equivalence circuit, where R_s, R_{ct}, C_{dl} and W are the resistance of solution, charge transfer resistance, double layer capacitance, and Warburg constant, respectively. The Fe_3O_4 NSs modified GCE (Fe_3O_4/GCE) shows a small R_{ct} value of 708 Ω due to its good conductivity as compared with R_{ct} value of 1224 Ω corresponding to Fe_3O_4@CuAl/GCE. The increased R_{ct} of Fe_3O_4@CuAl/GCE is due to deposition of

semiconductive CuAl LDH shell on Fe_3O_4 NS core, which hinders the fast electron transfer of interface to some extent. The electron transfer resistance of CuAl LDH modified GCE (CuAl/GCE) increased dramatically to 23280 Ω because of semiconductive properties of LDH materials, but still less than bare GCE with Rct of 3096 Ω, indicating fractional charge transfer ability due to the presence of holes within the layers of LDHs. These evidences indicate enhanced the electron transfer ability of Fe_3O_4@CuAl NSs owing to the synergistic effect of the Fe_3O_4 core wrapped by CuAl LDHs

To evaluate electrocatalytic performances of Fe_3O_4@CuAl/GCE to H_2O_2, the cyclic voltammetric (CV) measurements were performed in the absence and presence of 1 mM H_2O_2 in deoxygenated 0.1 M PBS (pH 7.4) (Fig. 4B). In the absence of H_2O_2, a pair of minor peaks which can be credited to iron phosphate redox of iron ions combined with phosphate ions in PBS (Zhang et al., 2008). When H_2O_2 was added, Fe_3O_4@CuAl/GCE exhibited an increased reduction peak at the potential of -0.70 V. By augmenting H_2O_2 concentrations in PBS, the reduction peak current densities also increased linearly (Fig. 4B inset). Electrocatalytic properties of as-prepared nonomaterial with varied loading of Cu in shell and CuAl LDH alone were also measured to compare their potential in H_2O_2 detection. Benefited from the synergistic effect of Fe_3O_4 NS core and CuAl LDH shell, the Fe_3O_4@CuAl/GCE exhibits enhanced the reduction current density at lower overpotential as compared to CuAl/GCE, as shown in Fig. 4C. Moreover, by increasing the deposition of CuAl LDH shell upto transitional composition of 18.96% copper loading on Fe_3O_4 NSs, the reduction peak current is increasing while reduction potential shifts negatively. Beyond intermediate composition, further increase in copper loading buried Fe_3O_4 core completely and resulted in lower reduction peak current with more negative potential (Fig. S2A). Unlike the CV curves for CuAl LDH and Fe_3O_4@CuAl NSs, Fe_3O_4 NSs catalyst has redox peaks which are attributed to the Fe(II)/Fe(III) redox couple. Compared with Fe_3O_4 NSs, Fe_3O_4@CuAl NSs shows well-defined reduction peak which is due to the charge transfer from Fe to CuAl LDH layers, consequently causes the slight modification in electronic structure of CuAl LDH in Fe_3O_4@CuAl NSs improving electrocatalysis significantly. Therefore, synergistic effect is proposed to arise from the partial electron transfer from Fe_3O_4 to CuAl LDH at nanoscale interface enhancing catalytic activity of as-prepared Fe_3O_4@CuAl NSs. The outstanding sensing performances of Fe_3O_4@CuAl NSs with 18.96% copper loading have been shown due to large surface area facilitating more surface active sites, the synergetic effect of

Fe_3O_4 NSs and CuAl LDHs and unique core-shell morphology which endows maximum interfacial effect between Fe_3O_4 core and CuAl shell.

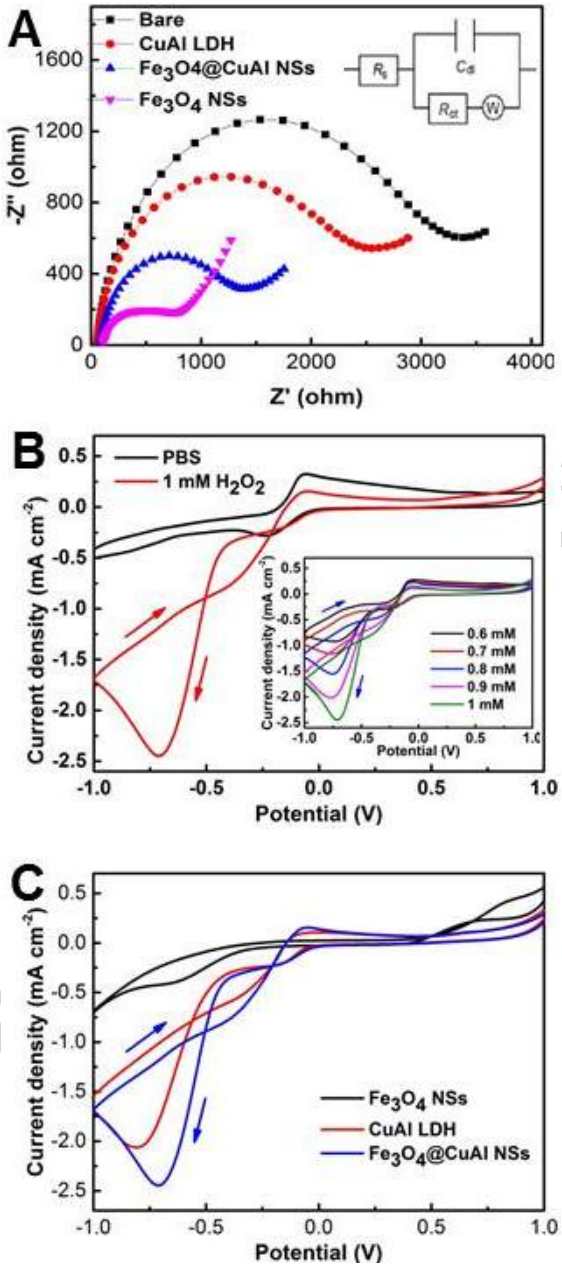

Fig. 4. (A) Nyquist plots of Fe_3O_4@CuAl/GCE, CuAl/GCE, Fe_3O_4/GCE and bare GCE in 0.1 M KCl consisting of 1.0 mM $K_3Fe(CN)_6$ and 1.0 mM $K_4Fe(CN)_6$. Frequency range: 0.1~10^5 Hz. Inset is the equivalent circuit. (B) Typical CV curves of Fe_3O_4@CuAl/GCE in N_2 saturated 0.1 M PBS in the absence (black line) and presence (red line) of 1 mM H_2O_2. Inset is the CV curves of Fe_3O_4@CuAl/GCE in 0.1 M PBS with different concentrations of H_2O_2. (C) CV curves of different nanohybrid electrodes in the presence of 1 mM H_2O_2 in 0.1 M PBS solution.

Amperometric measurements were applied to evaluate the sensitivity of Fe_3O_4@CuAl NSs upon successive additions of H_2O_2 concentration in stirring 0.1 M PBS (pH 7.4) at an applied potential of -0.70 V, as depicted by Fig. 5A and 5B. A rapid response was observed with the addition of 3 nM up to 10.05 mM H_2O_2, which achieve the steady-state current of ~95% within 3 s. This quick response of electrode can be credited to the fact that H_2O_2 being rapidly diffused and activated on active sites of highly rough surface created by the shell of LDH layers on Fe_3O_4@CuAl NSs as well as fast electron transfer kinetics. The real time detection limit with signal-to-noise factor of 3 (S/N=3) has also been evaluated by as-synthesized Fe_3O_4@CuAl/GCE, which is as low as 1 nM (Fig. 5C). These findings are superior than most of the H_2O_2 sensors reported in the literature published over the last year as depicted by Table S2. A broad linear range of reduction current density versus H_2O_2 concentration is presented by Fig. 5D. The curve exhibits three different linear responses in the range of 3~108 nM, 0.1~1.05 µM and 1.14~10052 µM with R^2 values of 0.995, 0.999 and 0.997 respectively. The phenomenon of reduction kinetics of catalytic processes is controlled by H_2O_2 absorption at extreme low concentration and by activation of H_2O_2 at high concentration, which is a rate-determining step, whereas in middle region the reduction current is controlled by combined effect of absorption and activation of H_2O_2 on electrode surface (Zhu et al., 2014).

The selectivity of proposed biosensor against potential interfering substance such as UA, AA, DA, glucose, nitrite has been evaluated at an applied potential of -0.70 V. As presented by Fig. 5E, the interferences upon the addition of 1 mM of interfering species were negligible at an applied detection potential, while the reduction current of 1 mM H_2O_2 reached its extreme value demonstrating preferable selectivity of resultant biosensor for the detection of H_2O_2. This excellent anti-interfering ability of Fe_3O_4@CuAl/GCE is due to negative operating potential that limits the oxidation of electroactive substances. The stability of Fe_3O_4@CuAl/GCE stored at room temperature was further investigated by recording the current responses of modified electrode to the reduction of 1 mM H_2O_2 which retained 95% of its initial current value up to 25 days of post preparation (Fig. 5F). To evaluate reproducibility of biosensor, six different glassy carbon electrodes were modified similarly with Fe_3O_4@CuAl NSs suspension and current responses of these electrodes were recorded with 1 mM H_2O_2 providing relative standard deviation (RSD) value less than 5%. A reproducible current with RSD less than 4% has also

been observed for six successive assays (Fig. 5F inset). These results authenticate the superb stability and reproducibility of proposed biosensor.

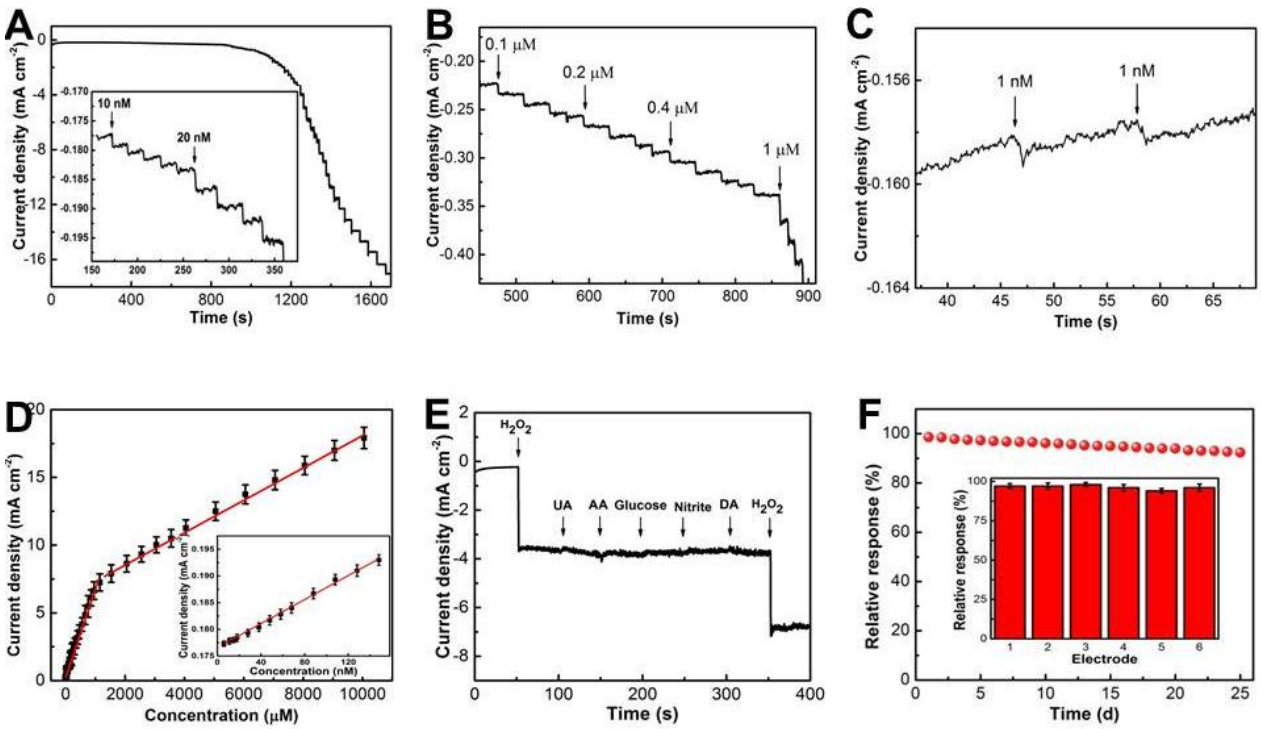

Fig. 5. (A) Amperometric responses of Fe_3O_4@CuAl/GCE with successive additions of different H_2O_2 concentrations in N_2 saturated 0.1 M PBS at -0.70 V. Inset is amperometric responses to 10 and 20 nM H_2O_2. (B) The closed look responses of Fe_3O_4@CuAl/GCE to several micromolars of H_2O_2. (C) Current responses for determining detection limit. (D) The calibration plot of current density *vs.* H_2O_2 concentration. (E) Anti-interference property with 1 mM addition of each electroactive species. (F) Time dependence responses with 1 mM H_2O_2. Inset is the current responses of six different electrodes to 1 mM H_2O_2.

3.3. In vitro tracking of H_2O_2 in biotic fluids

The life-threatening public health problem due to leading cause of cancer mortalities worldwide, the precise monitoring and potential therapy of such malignancy have attained wealth of attention. In this work, two different living cancer cell lines, *i.e.,* mouse hepatoma cell line H-22 and human hepatocellular carcinoma cell line BEL-7402 are chosen for real-time monitoring of H_2O_2 flux after being stimulated. And the bright-field images of these living cells are shown in Fig. 6A and 6D. BEL-7402 cell line is the fifth common malignancy, owing to

notoriously high chemoresistive and scarcity of effective therapy, it is ranked as third public issue of cancer related death (Zhang et al., 2014). The mouse liver cancer cell line H-22 is one of the common malignancies, at most five years of survival after its diagnosis, threatening seriously global public health with high mortality and mostly diagnosed after getting an advanced stage (Yang et al., 2014). The only way to improve resectability as well as survival rate and get rid of these lethal attacks is their early diagnosis. With marvelous sensitivity achieved the practical application of as synthesized Fe_3O_4@CuAl NSs modified electrode has been explored for real-time tracking of H_2O_2 released by different living cells and therapeutic efficacy of plasma medicines has also been assessed in cancer treatment by the proposed sensing platform. The endogenous H_2O_2 released was triggered by the addition of 0.1 mM fMLP. Upon the addition of 10 µL fMLP to the test wells, the significant reduction current densities of 0.121 mA cm^{-2} and 0.0891 mA cm^{-2} were observed in the presence of BEL-7402 and H-22 cells, respectively, as presented by Fig. 6B and 6E. Furthermore, current densities gradually decreased to a background level upon addition of catalase, indicating that released H_2O_2 is decomposed or diffused away from electrode in electrolytic solution. The control experiment without cells did not generate any detectable current signal, further suggesting that the triggered H_2O_2 efflux was due to stimulation of cells by fMLP (Fig. 6G).

Because of enhanced plasma chemistry, the therapeutic efficacy of PAM has been evaluated by detecting extracellular H_2O_2 released upon being stimulated by adding 10 µL of fMLP with proposed biosensor after plasma treatment. The significant decrease in current densities of 0.0334 mA cm^{-2}, 0.0088 mA cm^{-2} and 0.0196 mA cm^{-2}, 0.0068 mA cm^{-2} was observed for H-22 and BEL-7402 cell lines after being irradiated with plasma plumes for 1 min and 2 min, respectively (Fig. 6C and 6F), which decreased 72.39%, 92.15% and 78%, 91% in comparison to that without treatment (Fig. 6H). As manifested by plethora of plasma therapy experiments, that plasma consisting of OH, NO and NO_2 species interact with liquid to generate numerous ROS and RNS like H_2O_2, NO_2^-, NO_3^- which cause imbalancement of oxidants and antioxidants in living cells (Yan et al., 2012). The increased oxidative stress due to excessive production of H_2O_2 results in effective lipid peroxidation and ultimately triggers the cell death. Moreover, these species after diffusion into cells further interact with protein, DNA, RNA and switch on signal transduction as well as gene expression leading to induce cell death and change of cellular morphology (Tanaka et al., 2015). Therefore, most of living cancer cells die as

exposure time of plasma plumes increased from 1 to 2 min resulting in decrease of current densities caused by less secretion of H_2O_2 from cells. All these findings demonstrate the potential use of proposed biosensor for cancer diagnosis and enhanced therapeutic efficacy of plasma medicines for cancer treatments as well.

Additionally, H_2O_2 is a pathogenic factor for various diseases like kidney failure, parasitic infection and diabetes, so it is also necessary to monitor its exact level in human serum and urine samples (Chandramathi et al., 2009). Ultimately, endogenous amount of H_2O_2 from biofluids has been measured by as-synthesized biosensor based on Fe_3O_4@CuAl/GCE as presented by Fig. 6I-6K. The aliquots of serum and urine samples were inoculated into 15 mL of 0.1 M stirring PBS (pH 7.4) with subsequently spiking of some standard H_2O_2 concentrations. The ubiquitous amount of H_2O_2 excreted was determined by using regression equation and found the results for serum 12 µM, urine before 35.4 µM and after coffee intake 51.1 µM respectively. Considerable rise in urinary H_2O_2 level one hour after the intake of coffee has been noticed. Coffee beans are rich in hydroxy hydroquinone and polyphenols like chlorogenic acid, which is one possible cause of upsurge in urinary H_2O_2 concentration subsequently after coffee intake (Chatterjee and Chen, 2012). It can be concluded that these biological molecules are first absorbed into the body and then autoxidize upon exposure to oxygen, generating H_2O_2 after being excreted through urine. These results substantially demonstrate the reliable application of Fe_3O_4@CuAl NSs for cancer detection along with determination of ubiquitous H_2O_2 in biotic fluids.

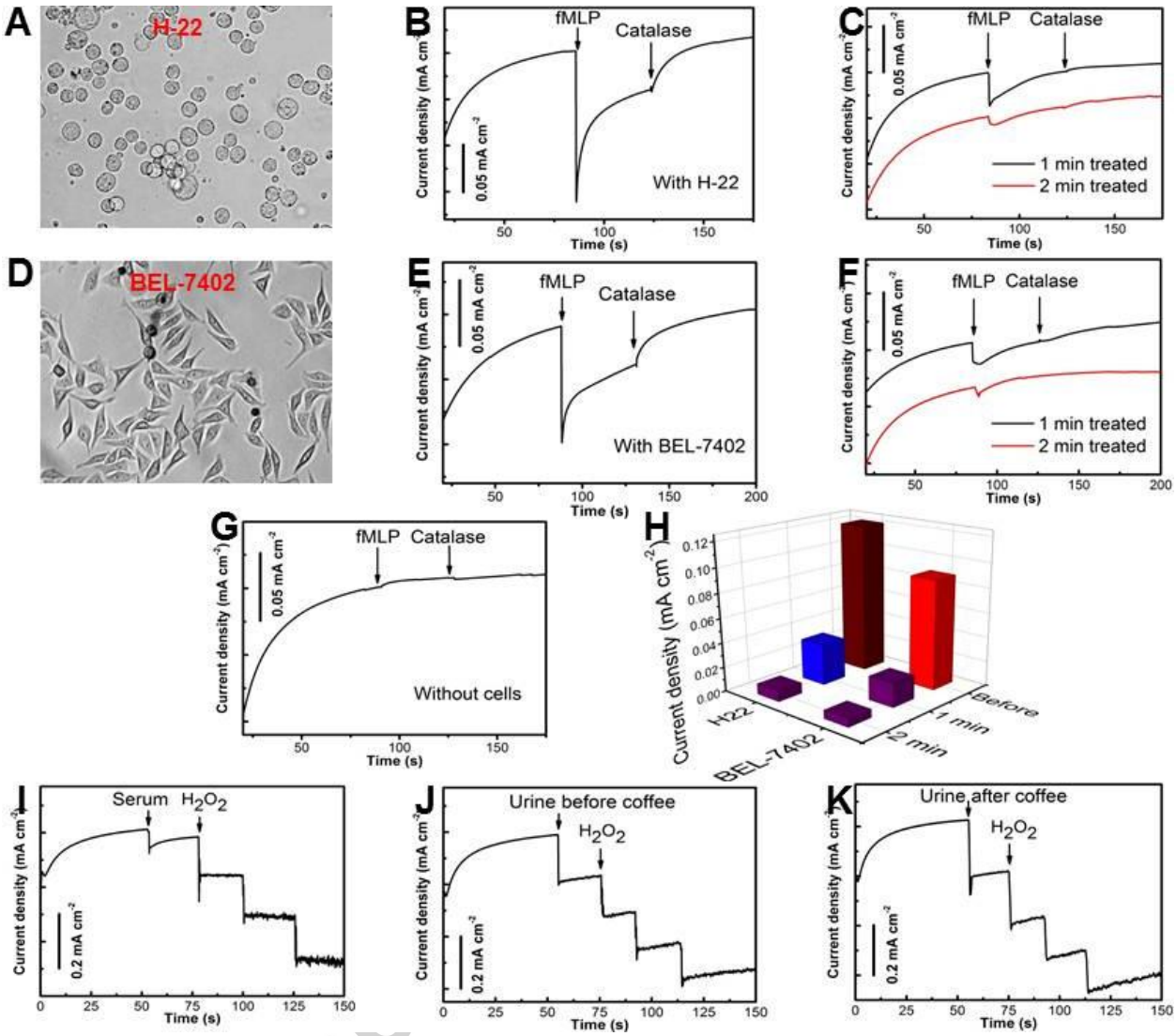

Fig. 6. Bright-field images of (A) H-22 cells, and (D) BEL-7402 cells. Amperometric responses of Fe_3O_4@CuAl/GCE upon the addition of 10 µL of fMLP in the tested wells with (B) H-22 cells, (E) BEL-7402 cells, and (G) without cells before plasma treatment, and (C) H-22 cells, and (F) BEL-7402 cells after 1 min (upper) and 2 min (lower) of plasma treatment, respectively. (H) Corresponding histogram of decreasing amperometric responses after plasma therapy. Amperometric responses of Fe_3O_4@CuAl/GCE upon an aliquot addition of (I) serum, and (J) and (K) urine prior and following to the intake of coffee by successive addition of 20 µM and 30 µM H_2O_2, respectively.

4. Conclusions

In summary, a novel hierarchical core-shell structured nanosphere hybrid material has been fabricated with controlled integration of p-type semiconductive nanosheets of CuAl LDHs functionalized on Fe_3O_4 NS core *via* facile, robust co-precipitation and hydrothermal approach. Arising from the drastic interfacial conduction, the synergistic effect derived from extraordinary intercalation features of LDHs shell and Fe_3O_4 NS core, and the abundant charge carriers, the resultant core-shell Fe_3O_4@CuAl NSs hybrid material exhibits enhanced electrocatalytic properties, The Fe_3O_4@CuAl NSs hybrid material based electrochemical biosensor has been deviced for quantification of H_2O_2 under biological environment which has exhibited high performance towards sensitive and specific H_2O_2 detection. The practical application of biosensor has been explored in detecting endogenous H_2O_2 concentrations in human serum and urine as well as *in vitro* detection of cancer and evaluating therapeutic efficacy of plasma irradiated medium in cancer therapy. Thus, our findings hold promising application potential in biosensing platform, pathological diagnostics and effectiveness of plasma in cancer therapy.

ASSOCIATED CONTENT

Supporting information available: Additional details, figures and tables as mentioned in the text. This material is available free of charge via Internet.

Notes

The authors declare no competing financial interest.

Acknowledgments

National Natural Science Foundation of China National Natural Science Foundation of China (No. 51572094), the Innovation Foundation of Huazhong University of Science (No. 2015TS150, 2015ZZGH010) and Technology and the Key Laboratory for Large-Format Battery Materials and System, ministry of Education and Fundamental Research Funds for the Central Universities (No. 2014QN110), We acknowledge the support of the Analytical and Testing Center of the Huazhong University of Science and Technology for SEM and XPS measurements.

References

Ai, F., Chen, H., Zhang, S.H., Liu, S.Y., Wei, F., Dong, X.Y., Cheng, J.K., Huang, W.H., 2009. Anal. Chem. 81, 8453-8458.

Al-Gaashani, R., Radiman, S., Tabet, N., Razak Daud, A., 2011. J. Alloys and Compounds 509, 8761-8769.

Asif, M., Aziz, A., Dao, A.Q., Hakeem, A., Wang, H., Dong, S., Zhang, G., Xiao, F., Liu, H., 2015. Ana. chim. acta 898, 34-41.

Asif, M., Haitao, W., Shuang, D., Aziz, A., Zhang, G., Xiao, F., Liu, H., 2017. Sens Actu. B: Chemical 239, 243-252.

Cardoso, A.R., Moreira, F.T., Fernandes, R., Sales, M.G., 2016. Biosens. Bioelectron. 80, 621-630.

Chandramathi, S., Suresh, K., Anita, Z.B., Kuppusamy, U.R., 2009. Parasitology 136, 359-363.

Chatterjee, S., Chen, A., 2012. Biosens. Bioelectron. 35(1), 302-307.

Chen, M., Hou, C., Huo, D., Bao, J., Fa, H., Shen, C., 2016. Biosens Bioelectron.

Ding, N., Yan, N., Ren, C., Chen, X., 2010. Anal. chem. 82, 5897-5899.

Ganesan, R., Lee, J.S., 2005. Angew. Chem. Int. Ed. 44, 6557-6560.

Han, X., Fang, K., Zhou, J., Zhao, L., Sun, Y., 2015. J. Coll. Inter. Sci.

Kaushik, N.K., Kaushik, N., Yoo, K.C., Uddin, N., Kim, J.S., Lee, S.J., Choi, E.H., 2016. Biomaterials 87, 118-130.

Keidar, M., 2012. Cold Atmosphere Plasma in Cancer Therapy. APS Meeting Abstracts, 2005.

Ko, Y.H., Nagaraju, G., Lee, S.H., Yu, J.S., 2014. Mat. Lett. 117, 217-220.

Li, C., Zhang, H., Wu, P., Gong, Z., Xu, G., Cai, C., 2011. Analyst 136, 1116-1123.

Liu, C.J., Yu, S.L., Liu, Y.P., Dai, X.J., Wu, Y., Li, R.J., Tao, J.C., 2016a. Eur. J. Med. Chem. 115, 26-40.

Luo, Y., Tian, Y., Rui, Q., 2009. Chem. Commun. 21, 3014-3016.

Maji, S.K., Sreejith, S., Mandal, A.K., Ma, X., Zhao, Y., 2014. ACS Appl. Mater. Interfaces 6, 13648-13656.

Senapati, S., Thakur, R., Verma, S.P., Duggal, S., Mishra, D.P., Das, P., Shripathi, T., Kumar, M., Rana, D., Maiti, P., 2016. J. Control Release 224, 186-198.

Shen, W., Yang, C., Bao, X., Sun, L., Wang, N., Tang, J., Chen, W., Yang, R., 2015. Mat. Sci. Eng. B 200, 1-8.

Song, S., Yang, H., Rao, R., Liu, H., Zhang, A., 2010. App. Catal. A: General 375, 265-271.

Tanaka, H., Mizuno, M., Ishikawa, K., Kondo, H., Takeda, K., Hashizume, H., Nakamura, K., Utsumi, F., Kajiyama, H., Kano, H., Okazaki, Y., Toyokuni, S., Akiyama, S.i., Maruyama, S., Yamada, S., Kodera, Y., Kaneko, H., Terasaki, H., Hara, H., Adachi, T., Iida, M., Yajima, I., Kato, M., Kikkawa, F., Hori, M., 2015. Clin. Plasma Medicine 3, 72-76.

Von Woedtke, T., Metelmann, H.R., Weltmann, K.D., 2014. Contri. Plas. Phy. 54, 104-117.

Wang, Y., Peng, W., Liu, L., Gao, F., Li, M., 2012. Electrochim. Acta 70, 193-198.

Wang, Z., Chen, M., Shu, J., Li, Y., 2016b. J. Alloys and Compounds 682, 432-440.

Weinstain, R., Savariar, E.N., Felsen, C.N., Tsien, R.Y., 2014. J. Am. Chem. Soc. 136, 874-877.

Williams, M.J., Sánchez, E., Aluri, E.R., Douglas, F.J., MacLaren, D.A., Collins, O.M., Cussen, E.J., Budge, J.D., Sanders, L.C., Michaelis, M., 2016. RSC Advances 6, 83520-83528.

Wu, P., Cai, Z., Chen, J., Zhang, H., Cai, C., 2011. Biosens. Bioelectron. 26, 4012-4017.

Xi, J., Xie, C., Zhang, Y., Wang, L., Xiao, J., Duan, X., Ren, J., Xiao, F., Wang, S., 2016. ACS App. Mater. Interfaces 8, 22563-22573.

Xi, J., Zhang, Y., Wang, N., Wang, L., Zhang, Z., Xiao, F., Wang, S., 2015. ACS Appl. Mater. Interfaces 7, 5583-5590.

Xu, Z., Yang, L., Xu, C., 2015. Anal. Chem. 87, 3438-3444.

Yahalom, G., Weiss, D., Novikov, I., Bevers, T.B., Radvanyi, L.G., Liu, M., Piura, B., Iacobelli, S., Sandri, M.T., Cassano, E., 2013. Biomark. cancer 5, 71.

Yan, L.G., Yang, K., Shan, R.R., Yan, T., Wei, J., Yu, S.J., Yu, H.Q., Du, B., 2015. J. Coll. Inter. Sci. 448, 508-516.

Yan, X., Xiong, Z., Zou, F., Zhao, S., Lu, X., Yang, G., He, G., Ostrikov, K.K., 2012. Plas. Processes and Polymers 9, 59-66.

Yang, J., Li, X., Xue, Y., Wang, N., Liu, W., 2014. Int. J. Biol. Macromol. 64, 276-280.

Yin, X., Guo, M., Xia, Y., Huang, W., Li, Z., 2014. J. Electroanal. Chem. 720-721, 19-23.

Yu, C., Wang, L., Li, W., Zhu, C., Bao, N., Gu, H., 2015. Sens. Actu. B: Chemical 211, 17-24.

Yuan, M., Liu, A., Zhao, M., Dong, W., Zhao, T., Wang, J., Tang, W., 2014. Sens. Actu. B: Chemical 190, 707-714.

Zhang, L., Zhai, Y., Gao, N., Wen, D., Dong, S., 2008. Electrochem. Commun. 10, 1524-1526.

Zhang, Z., Zhang, C., Ding, Y., Zhao, Q., Yang, L., Ling, J., Liu, L., Ji, H., Zhang, Y., 2014. Food Chem. Toxicol. 63, 38-47.

Zhu, H., Sigdel, A., Zhang, S., Su, D., Xi, Z., Li, Q., Sun, S., 2014. Angew. Chem. Int. Ed. 126, 12716-12720.

Zhu, L., Zhang, Y., Xu, P., Wen, W., Li, X., Xu, J., 2016. Biosens. Bioelectron. 80, 601-606.

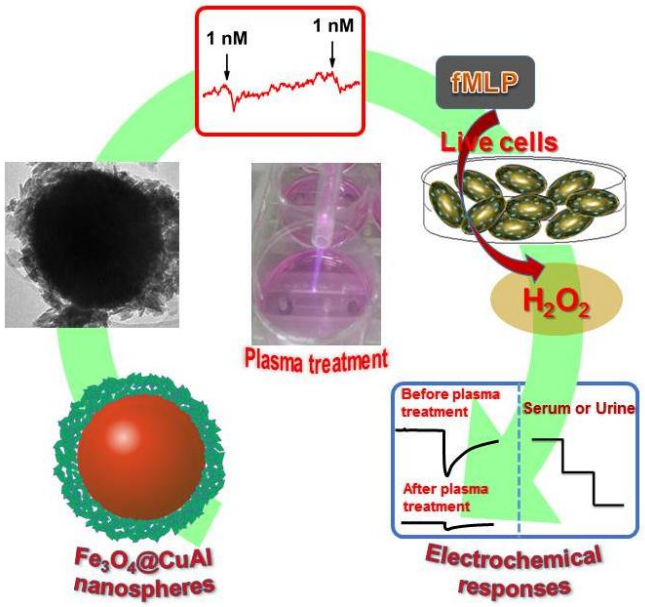

TOC

Highlights

- Core-shell Fe_3O_4@CuAl NSs have been synthesized by hydrothermal and co-precipitation approach.
- Fe_3O_4@CuAl NSs electrode exhibits marvelous electrochemical performance towards the nonenzymatic sensing of H_2O_2.
- Real-time monitoring of H_2O_2 from blood serum, urine and secreted by various live cancer cells before and after treatment.
- Atmospheric pressure plasmas have been used as potential therapeutic approach for cancer therapy.